NACA RM A50E26

NACA

RESEARCH MEMORANDUM

INVESTIGATION AT HIGH SUBSONIC SPEEDS OF METHODS OF ALLEVIATING THE ADVERSE INTERFERENCE AT THE ROOT OF A SWEPT-BACK WING

By Lee E. Boddy

Ames Aeronautical Laboratory
Moffett Field, Calif.

NATIONAL ADVISORY COMMITTEE
FOR AERONAUTICS

WASHINGTON

August 10, 1950

NATIONAL ADVISORY COMMITTEE FOR AERONAUTICS

RESEARCH MEMORANDUM

INVESTIGATION AT HIGH SUBSONIC SPEEDS OF METHODS OF ALLEVIATING THE ADVERSE INTERFERENCE AT THE ROOT OF A SWEPT-BACK WING

By Lee E. Boddy

SUMMARY

Interference at the root of a swept-back wing was investigated at high subsonic Mach numbers by means of wind-tunnel measurements of a wing-body combination having the 50-percent-chord line of the wing either unswept or swept back 35°. Modifications to the body contour and to the wing-root profile designed to alleviate the small interference of the swept configuration were evaluated by force and pressure-distribution measurements.

Below the Mach number for drag divergence, the pressure distribution at the midsemispan of the swept-back wing was accurately predicted from results of the tests of the unswept wing using the simple cosine concepts. Furthermore, about 90 percent of the predicted increase of drag-divergence Mach number was realized experimentally from the sweepback of the model wing, the measured divergence Mach number being about 0.015 lower than the predicted divergence Mach number. Most of this small deficiency appeared to be overcome by the modifications to the body contour or to the wing-root profile, either of which increased the drag-divergence Mach number of the model with the swept-back wing approximately 0.01.

INTRODUCTION

The substantial benefits of sweeping the wings of airplanes to delay the onset of compressibility effects have been demonstrated with wind-tunnel and flight tests. However, in many instances the benefits were not as great as anticipated from consideration of simple sweep concepts. Some of the wind-tunnel tests revealed that the premature compressibility effects might be the result of unfavorable flow conditions near the root of the swept-back wing, and indicated the necessity for more detailed tests to investigate the problem.

The investigation reported herein consisted of a study of the flow over a swept-back wing compared to that over an unswept wing, and a determination of the effects of altering the flow at the root of the swept-back wing. Two methods of altering the flow at the wing root were employed, both designed to provide a pressure distribution at the wing-body juncture similar to that near the midsemispan of the wing. These methods were: (1) contouring the body sides to conform to the estimated shape of the streamlines over the midsemispan of the wing, and (2) changing the profile at the root of the wing.

NOTATION

The coefficients and symbols used in this report are defined as follows:

C_D drag coefficient $\left(\frac{\text{drag}}{qS}\right)$

C_L lift coefficient $\left(\frac{\text{lift}}{qS}\right)$

C_m pitching-moment coefficient $\left(\frac{\text{pitching moment}}{qS\bar{c}}\right)$

M free-stream Mach number

P pressure coefficient $\left[\frac{(\text{local static pressure})-(\text{free-stream static pressure})}{q}\right]$

S wing area, square feet

V free-stream velocity, feet per second

b wing span, feet

c local wing chord, feet

$\bar{c}$ wing mean aerodynamic chord $\left(\frac{\int_0^{b/2} c^2\,dy}{\int_0^{b/2} c\,dy}\right)$, feet

c_r wing root chord, feet

c_t wing tip chord, feet

q free-stream dynamic pressure $\left(\frac{1}{2}\rho V^2\right)$, pounds per square foot

x	distance behind wing leading edge, feet
y	lateral distance from model center line, feet
α	angle of attack of fuselage center line, degrees
ρ	free-stream mass density, slugs per cubic foot

APPARATUS AND MODEL

The tests were conducted in the Ames 16-foot high-speed wind tunnel, with the model mounted on a sting support as shown in figure 1. Lift, drag, and pitching moment were measured with electrical strain gages enclosed by the model.

Model Geometry

The model was constructed so that the wing could be tested with the 50-percent-chord line either unswept (fig. 2) or swept back 35° (fig. 3), and had removable panels on both the wing and the body near the wing-body juncture. Unswept, the wing had an aspect ratio of 9.0, a taper ratio of 0.5, and NACA 64A015 sections normal to the 50-percent-chord line. Swept back 35°, the wing had an aspect ratio of 6.0. In both cases the model wing area was 4.131 square feet. The mean aerodynamic chord was 0.700 foot for the unswept wing and 0.857 foot for the swept-back wing. Without modification, the body had a cylindrical midsection (herein called straight-sided body) and a nose of sufficient length to keep the major body-induced velocities well ahead of the wing.

The model has 12 chordwise rows of pressure orifices distributed over the upper surface of the right wing (indicated by the dots in figs. 2 and 3), five chordwise rows on the lower surface of the right wing, and a single row along the side of the body just above the wing. All orifices were connected to multiple mercury manometers by means of flexible tubing. Photographs of the manometers provided records of the pressures.

Model Modifications

The removable panels on the wing and body were designed to permit modifications to the model in order to alter the flow near the wing-body juncture. Two separate modifications were employed (fig. 4), each designed to provide a pressure distribution at the wing-body juncture similar to that near the midsemispan of the wing. These modifications

were: (1) contouring the body sides to conform to the estimated shape of the streamlines over the midsemispan of the wing, and (2) changing the profile at the root of the wing.

Contoured body.- References 1 and 2 suggest methods of contouring bodies and nacelles to minimize their interference with the flow over swept wings. The body shown in figure 4(a) was contoured using the method of reference 1, which suggests that a body on an infinite oblique wing should conform to the natural shape of the streamlines over the wing. The method presented in reference 1 for determining the streamline pattern over the oblique wing utilized the simple cosine concepts of oblique flows. Thus, the streamlines that form the desired body shape shown in figure 4(a) were ascertained by combining the uniform flow component parallel to the sweep axis (50-percent-chord line) with the flow field in the midsemispan plane perpendicular to the sweep axis. This latter flow field was determined by assuming it to be two-dimensional and using the method of reference 3. The assumption is warranted because the wing aspect ratio is sufficiently large and computations were made only for zero lift. The flow field was then adjusted for compressibility by the Prandtl-Glauert method to a Mach number of 0.70 (corresponding to a free-stream Mach number of 0.85 for the swept-back wing). The streamline shapes were calculated for several distances above and below the wing and were applied to the body lines in such a manner that, within the limits of the body depth, the intersection of the body with any horizontal plane had the same shape as the intersection of that plane with the calculated streamline pattern.

Modified wing-root profile.- It was known qualitatively that the lateral confinement of the streamlines near the center section of a swept-back wing decreased the velocity over the forward portion of the chord and increased the velocity over the rear portion of the chord (reference 4). To counteract these interference velocities, then, the wing-root profile would have to be modified to have higher velocities forward and lower velocities aft. The NACA 0015 section satisfied this requirement, especially over the forward half of the chord. Hence, at the intersection of the wing-chord plane and the straight-sided body, the modified wing profile was the NACA 0015 reduced in thickness to that of the basic airfoil in the stream direction. (See fig. 4(b).) The wing profile was faired linearly to the basic airfoil 0.45 root-chord length outboard of the juncture. (See fig. 3.)

REDUCTION OF DATA

The lift, drag, and pitching moment were reduced to coefficient form using the model wing area of 4.131 square feet and the wing mean aerodynamic chord of 0.700 foot for the unswept wing and 0.857 foot for the 35° swept-back wing. All pitching moments were referred to an axis passing through the 25-percent point of the wing mean aerodynamic chord. (See figs. 2 and 3.)

The test Reynolds number, based on the wing mean aerodynamic chord, varied from 2.6 million at 0.50 Mach number to 3.5 million at 0.94 Mach number for the swept-back wing, and was smaller for the unswept wing by the ratio of the mean aerodynamic chords.

Wind-tunnel-wall corrections to the angle of attack and drag coefficient, computed by the method of reference 5, were as follows:

$$\Delta\alpha \text{ (deg)} = 0.22\ C_L$$

$$\Delta C_D = 0.00384 C_L^2$$

Constriction effects of the wind-tunnel walls on the test Mach numbers (computed by the method of reference 6) were taken into account and amounted to about 1-1/2 percent at 0.94 Mach number.

It is believed that the drag coefficients shown in this report are slightly in error due to balance interaction discovered subsequent to the tests. The absolute values of the drag coefficients should not be compared, since the error in the drag readings was a function of the lift and pitching moment of the model and also appeared to vary slightly with time. However, the measured values of drag-divergence Mach number are believed to be reliable.

RESULTS AND DISCUSSION

Body Characteristics

The pressure distribution on the side of the body with the wing removed (fig. 5) shows that the root of the swept-back wing was well behind the major velocities induced by the straight-sided body. In fact, the nose of the body could be shortened as much as 7 inches and the body-induced velocities in the region of the wing root still would be very small.

Figure 6 presents the aerodynamic characteristics of the body with the wing removed, based on the model wing area and mean aerodynamic chord. The pitching-moment data for the straight-sided body were reduced using the mean aerodynamic chord and the moment-center position for both the unswept wing and the swept-back wing. It should be noted that the drag coefficients shown for the body are small and in some cases are slightly negative. This is due largely to the fact that only the forces on the forebody were measured, the afterbody being attached to the sting support as shown in figures 2 and 3. Furthermore, the absolute values of the drag coefficient are believed to be slightly in error due to interaction of lift and pitching moment affecting the drag readings.

Pressure Studies

Figure 7 shows the distributions of pressure coefficient at three different sections on the 35° swept-back wing. Note the rearward displacement of the minimum pressures near the root and the forward displacement near the tip. Also shown in figure 7 is the pressure distribution predicted for the midsemispan station of the swept wing from results of tests of the unswept wing using the simple cosine concept. The data from the tests of the unswept wing were converted to those for a swept wing by dividing the Mach number by the cosine of the sweep angle, multiplying the pressure coefficient by the square of the cosine of the sweep angle, and multiplying the angle of attack by the cosine of the sweep angle. Good agreement was obtained at all Mach numbers below that for drag divergence ($\partial C_D/\partial M=0.10$); whereas at higher Mach numbers the agreement was only fair. It should be mentioned that pressures on swept and unswept lifting surfaces would be expected to be comparable in this manner only near the midsemispan, since, for the same total lift, the swept-back wing has more lift near the tip and less lift near the root than the unswept wing.

The foregoing is fairly strong evidence that the portions of the swept-back wing near the midsemispan behaved much as would be predicted by the simple cosine concept, except, of course, for the different boundary-layer effects. It was reasoned, then, that any failure of the wing to realize the full benefits of sweepback would probably occur near the root or tip sections, and altering the pressure distribution at the wing root to conform with that at the midsemispan might be beneficial.

In figure 8 are shown the chordwise pressure distributions near the wing root for the basic model and for the model with the two modifications. Also, shown by the dotted line is the pressure distribution for the midsemispan station. It was intended that, by the modifications, this distribution be maintained over the inner portion of the wing. At small angles of attack the effect of the contoured body was about as had been calculated, except that the magnitude of the effect was only about half as great as desired; that is, the pressures with the contoured body were about midway between those for the straight-sided body and those at the midsemispan. This deficiency may have been due in part to the fact that, theoretically, the modification should extend a considerable distance above and below the wing before its effect becomes negligible; whereas on the model it was limited by the depth of the body. The effect of the modified wing-root profile on the pressure distribution consisted largely of a reduction of the velocities over the middle portion of the chord. The effects of body modification and wing-root modification are reflected in the pressure-contour plots shown in figures 9 to 11. Note that the pressure contours with the contoured body were generally straighter and were not displaced rearward near the root as much as with the straight-sided body. Also, the modified wing root substantially reduced the velocities near the midchord in the region of the wing-body juncture.

Tuft Studies

The results of tuft studies shown on the left wing panels in figures 9 to 11 revealed no consistent effects of the modifications, although, in general, the flow above the divergence Mach number appeared to be somewhat steadier with the modifications. In any case, the flow at the wing–body juncture remained steady, the regions of disturbed flow occurring on the midsemispan or tip portions of the wing.

Force Studies

Figures 12 to 15 present the aerodynamic force and moment characteristics of the various configurations. Figure 16 is a summary of the force characteristics of the model with the unswept wing and with the 35° swept–back wing. Either of the modifications to the model with the swept–back wing appeared to increase the Mach number for drag divergence approximately 0.01. Of particular interest is the fact that application of the simple cosine concept to the drag–divergence Mach number of 0.74 for the unswept wing at zero lift results in a predicted drag–divergence Mach number of 0.90 for the 35° swept–back wing, a value which agrees very well with that measured for the model with either of the modifications. Thus it appears that the gain from the modifications, although small, was about as much as could be expected with this model. Even the model without the modifications had about 90 percent of the predicted increase of divergence Mach number due to sweeping the wings.

Attention is called to two factors which bear heavily on the foregoing assessment of the benefits of the sweepback and of the modifications. First is the fact that the shape–induced velocities near the critical region of the wing–body juncture (fig. 9(a)) were slightly less than those over the major portion of the wing, possibly because the body was shaped to induce no velocity in this region and its depth was small enough to allow relief similar to that at the wing tips. This decrease of induced velocity effectively increased the critical Mach number of the wing–body juncture. The second factor is the determination of the proper axis upon which to base the angle of sweepback for a tapered wing. For example, if the sweep of the 25–percent–chord line (37.1°) were used in the foregoing analysis, a drag–divergence Mach number of 0.925 would be predicted for the swept–back wing, and one would conclude that the gain from the sweepback was only about 80 percent of the predicted value. However, for the purpose of predicting characteristics which are primarily dependent upon shock formation, it is believed preferable to use an axis parallel to the shock front. At zero lift the shock front of an infinite–span wing with the NACA 64A015 section would be expected to develop slightly behind the 40–percent–chord line. Also, the contours of figure 9(a) indicate that the shock at the midsemispan developed at between 40 and 60 percent of the chord. Thus it appears for the present case

that the 50-percent-chord line is a valid axis upon which to base the angle of sweepback.

An attempt was made to substantiate qualitatively the increase of drag-divergence Mach number realized from the modifications by computing from pressure measurements the wing pressure-drag coefficient near the wing-body juncture. The results of these computations are presented in figure 17. It should be noted that the data shown for the model with the straight-sided body are a true representation of the pressure drag in the region of the juncture since the straight-sided body could have no pressure drag in this region. However, the contoured body, with some of its surface sloping relative to the drag direction, could experience pressure drag near the juncture, but this drag was not evaluated because of the limited instrumentation. The large decrease of wing pressure drag shown at 0.60 Mach number for the model with the contoured body is probably counteracted to some extent by a pressure drag on the body itself. When only the valid comparison is made for the model with the straight-sided body, then, it is revealed that the modified root profile reduced the pressure drag of the wing-body juncture considerably at high Mach numbers. It appears that the primary effect of the modification was to maintain the subsonic character of the flow in the juncture at a higher free-stream Mach number.

CONCLUDING REMARKS

Below the Mach number for drag divergence, the pressure distribution at the midsemispan of the wing having its 50-percent-chord line swept back 35° was accurately predicted from tests of the unswept wing using the simple cosine concepts.

About 90 percent of the predicted increase of drag-divergence Mach number was realized experimentally from the sweepback of the model wing, the measured divergence Mach number being about 0.015 lower than the predicted divergence Mach number. Most of this small deficiency appeared to be overcome by the modifications to the body contour or to the wing-root profile, either of which increased the drag-divergence Mach number of the model with the swept-back wing approximately 0.01.

Modifying the profile at the root of the swept-back wing decreased the pressure drag of the wing root at high subsonic Mach numbers.

Ames Aeronautical Laboratory,
National Advisory Committee for Aeronautics,
Moffett Field, Calif.

REFERENCES

1. Watkins, Charles E.: The Streamline Pattern in the Vicinity of an Oblique Airfoil. NACA TN 1231, 1947.

2. Kuchemann, D.: Design of Wing Junction, Fuselage and Nacelles to Obtain the Full Benefit of Swept-Back Wings at High Mach Number. Rep. No. Aero. 2219, R.A.E. (British), 1947.

3. Jones, Robert T., and Cohen, Doris: A Graphical Method of Determining Pressure Distribution in Two-Dimensional Flow. NACA Rep. 722, 1941.

4. Neumark, S.: Velocity Distribution on Straight and Swept-Back Wings of Small Thickness and Infinite Aspect Ratio at Zero Incidence. Rep. No. Aero 2200, R.A.E. (British), 1947.

5. Silverstein, Abe, and White, James A.: Wind-Tunnel Interference with Particular Reference to Off-Center Positions of the Wing and to the Downwash at the Tail. NACA Rep. 547, 1935.

6. Herriot, John G.: Blockage Corrections for Three-Dimensional-Flow Closed-Throat Wind Tunnels, with Consideration of the Effect of Compressibility. NACA RM A7B28, 1947.

(a) Lower front view of model with swept-back wing.

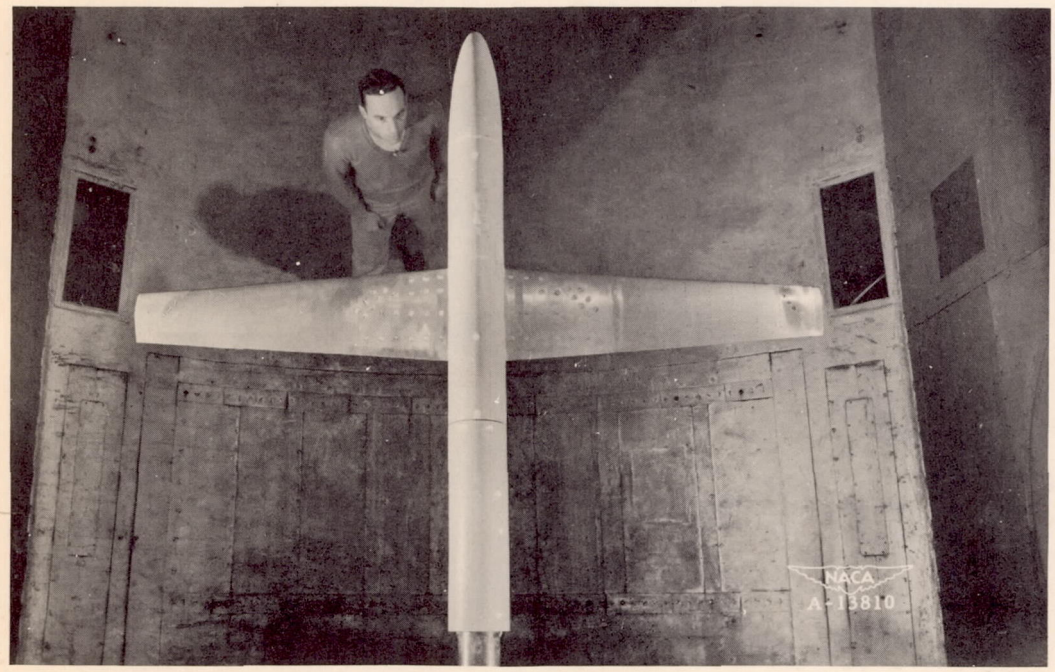

(b) Top view of model with unswept wing.

Figure 1.- Photographs of the model mounted in the wind-tunnel test section.

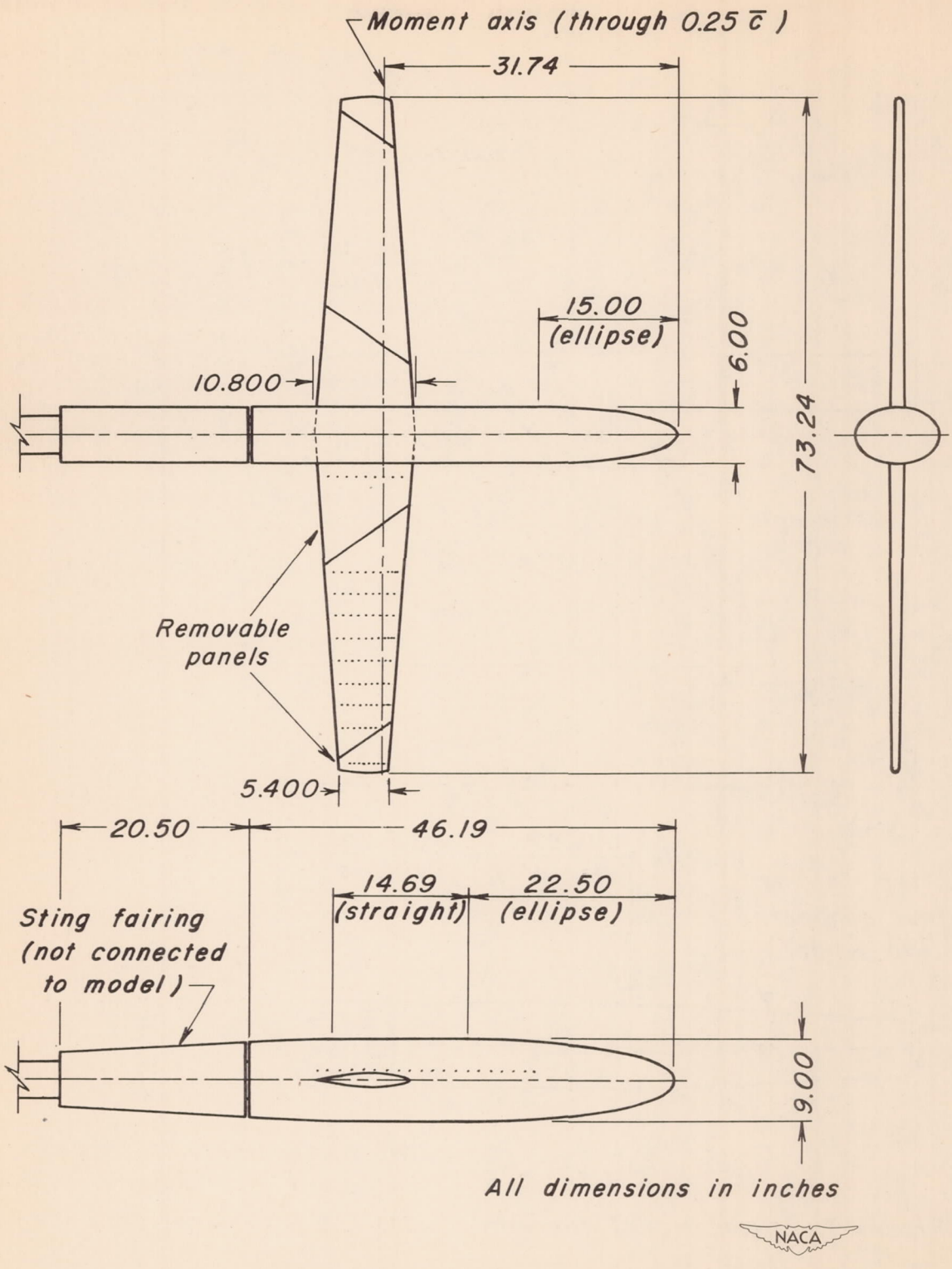

Figure 2.- Geometry of the model with the unswept wing.

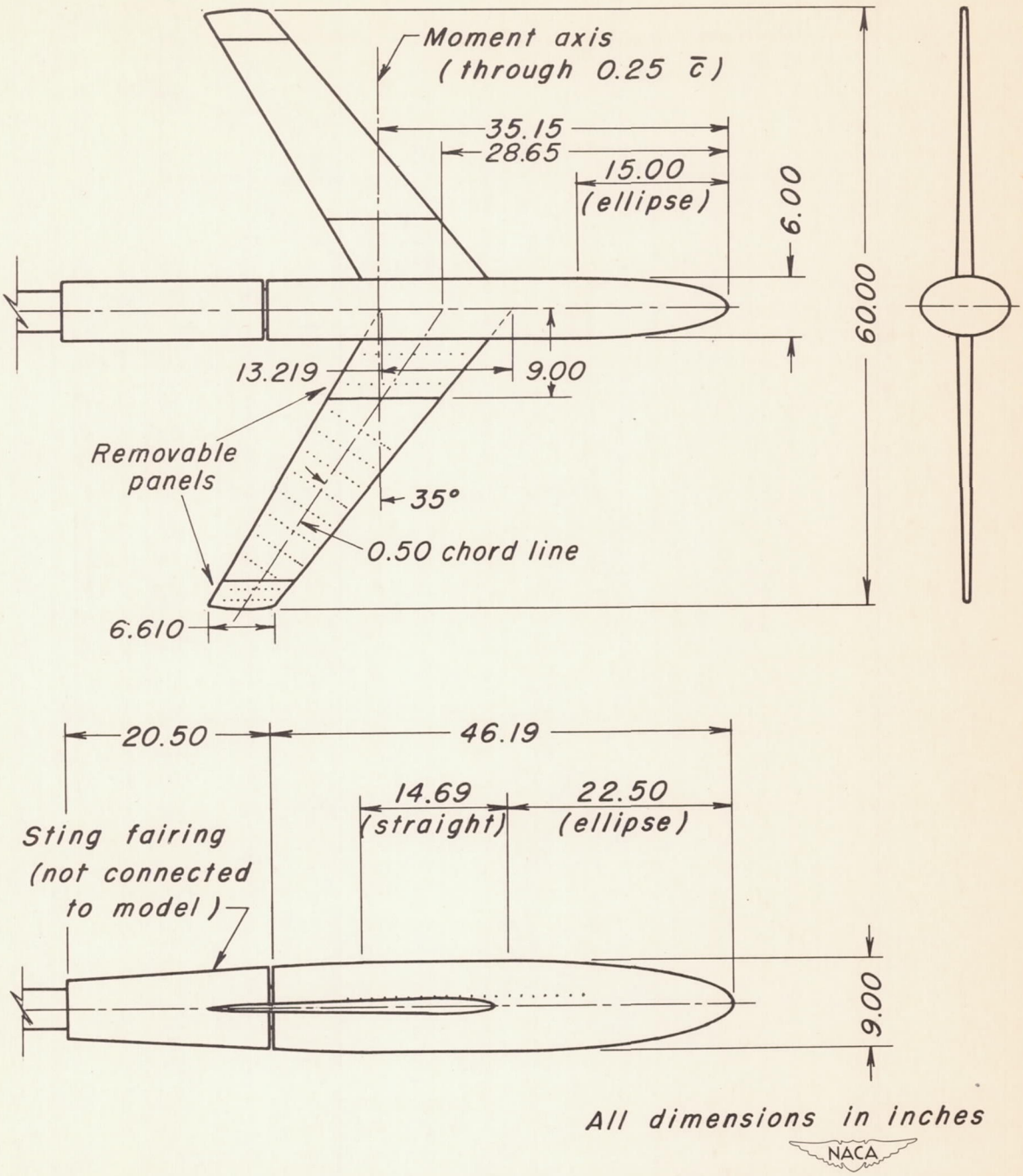

Figure 3.– Geometry of the model with the 35° swept-back wing.

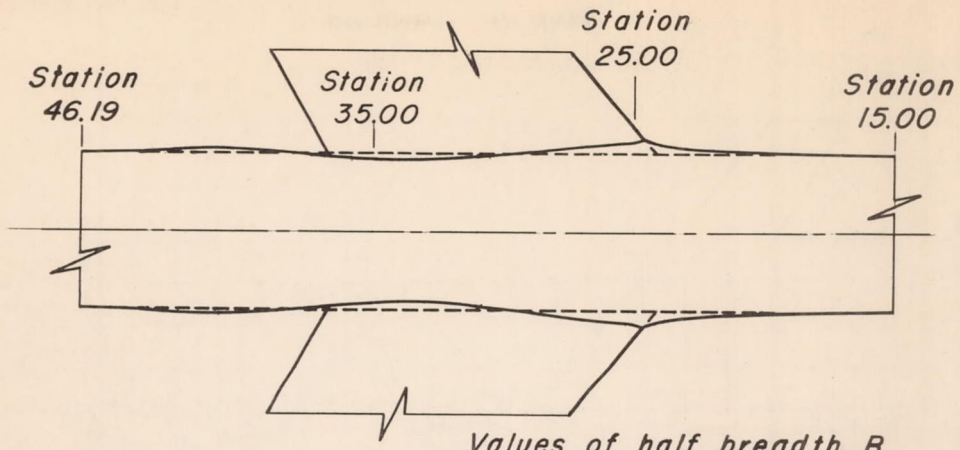

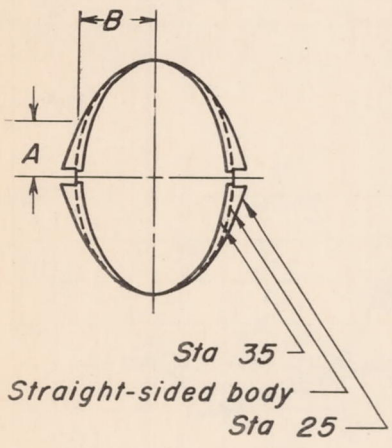

Typical sections

All dimensions in inches

Values of half breadth, B

Fuselage Station	Half height, A					
	0.00	0.50	1.00	2.00	3.00	4.00
15.00	3.00	2.98	2.91	2.64	2.12	0.98
19.00	3.10	3.07	3.00	2.74	2.26	1.34
21.00	3.16	3.10	3.03	2.78	2.30	1.40
23.00	3.26	3.21	3.13	2.83	2.34	1.43
24.00	3.41	3.32	3.21	2.87	2.36	1.44
25.00	3.66	3.45	3.27	2.88	2.34	1.42
27.00	3.60	3.38	3.21	2.82	2.28	1.37
29.00	3.26	3.14	3.01	2.68	2.19	1.30
31.00	2.96	2.91	2.84	2.55	2.07	1.20
33.00	2.80	2.77	2.71	2.45	2.00	1.15
35.00	2.80	2.75	2.67	2.41	1.98	1.14
37.00	2.91	2.84	2.74	2.45	1.98	1.13
39.00	3.10	2.92	2.80	2.48	2.00	1.12
41.00	3.20	2.97	2.85	2.53	2.02	1.07
43.00	3.10	2.99	2.88	2.57	2.06	1.00
46.19	3.00	2.98	2.92	2.64	2.12	0.97

(a) Geometry of contoured body.

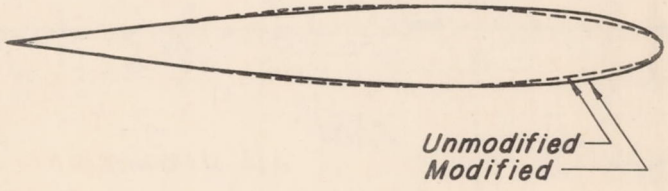

(b) Modified wing—root profile.

Figure 4. – Geometry of the model modifications.

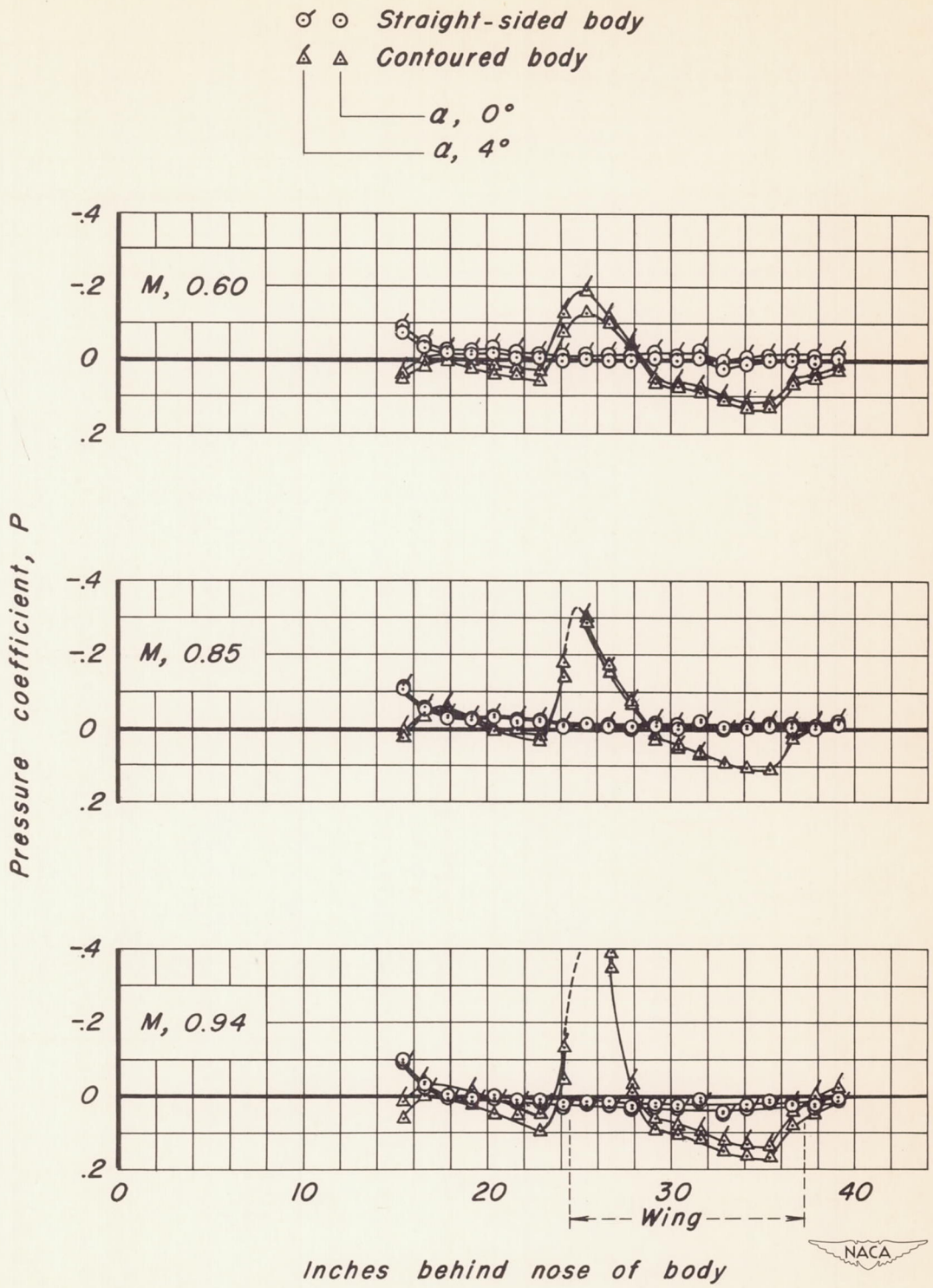

Figure 5.- Pressure distribution on the side of the body with the wing removed.

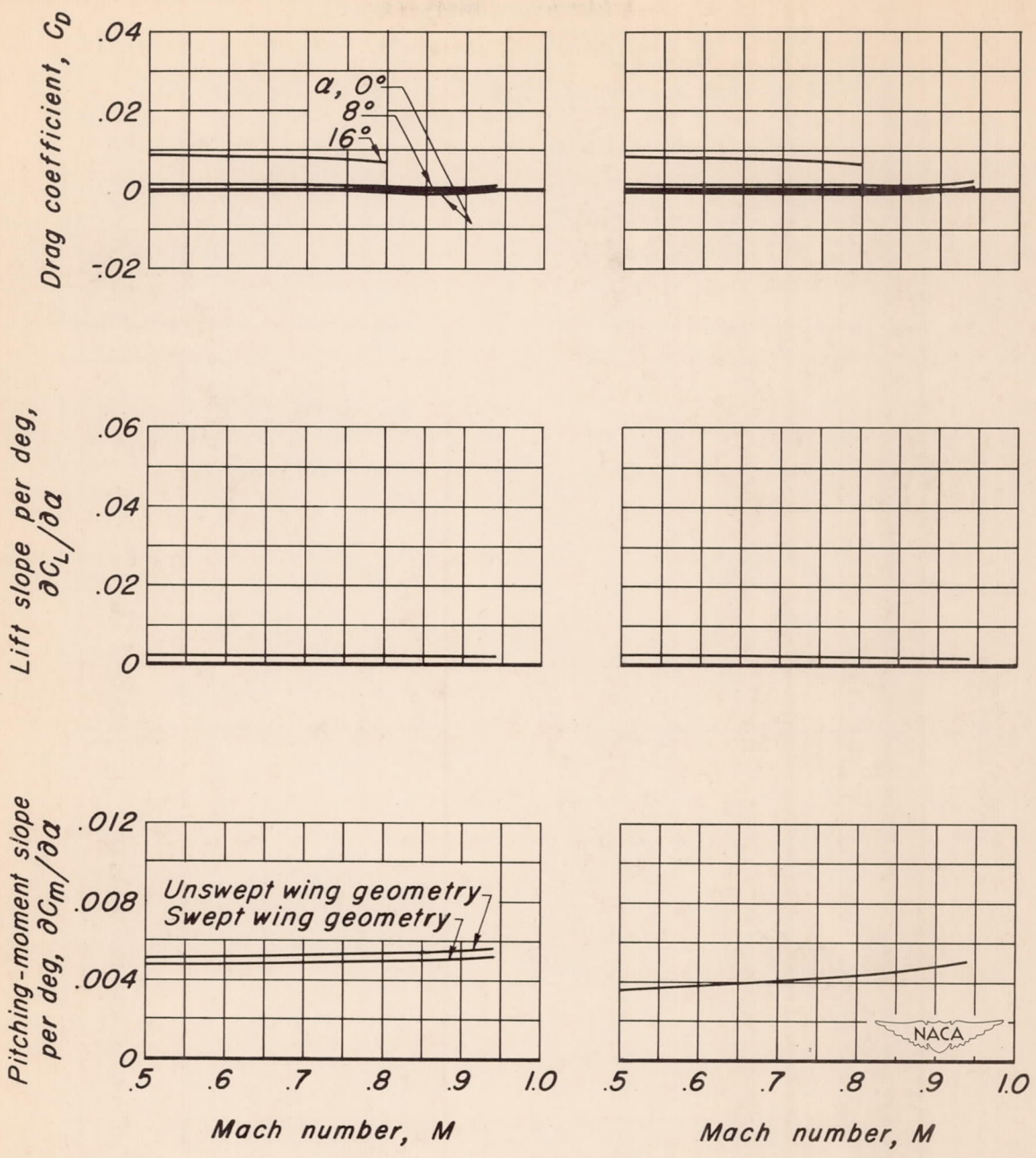

(a) Straight-sided body. (b) Contoured body.

Figure 6.- Aerodynamic characteristics of the body with the wing removed.

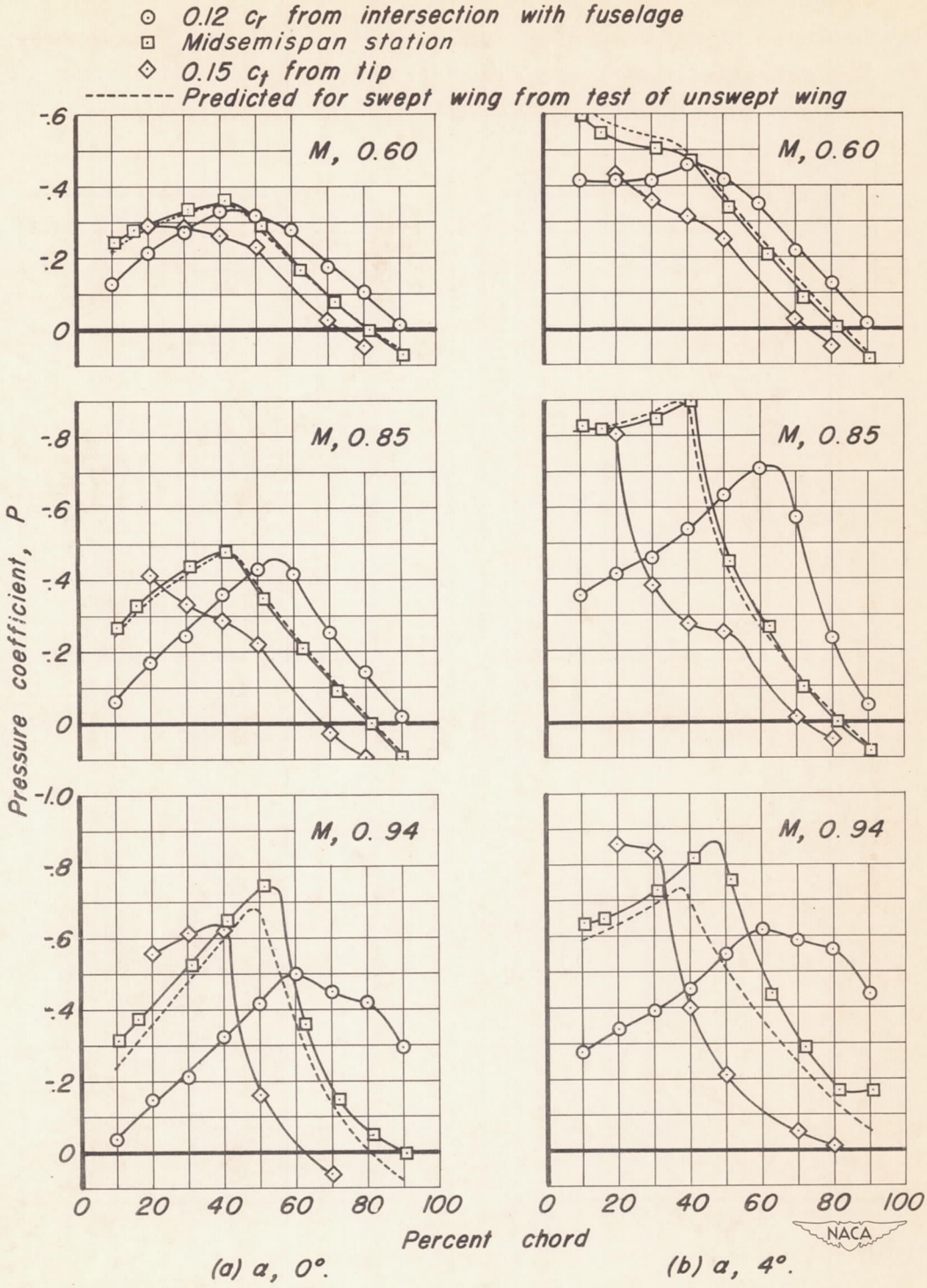

Figure 7.- Pressure distribution on the upper surface of the swept wing with straight-sided fuselage, unmodified root profile.

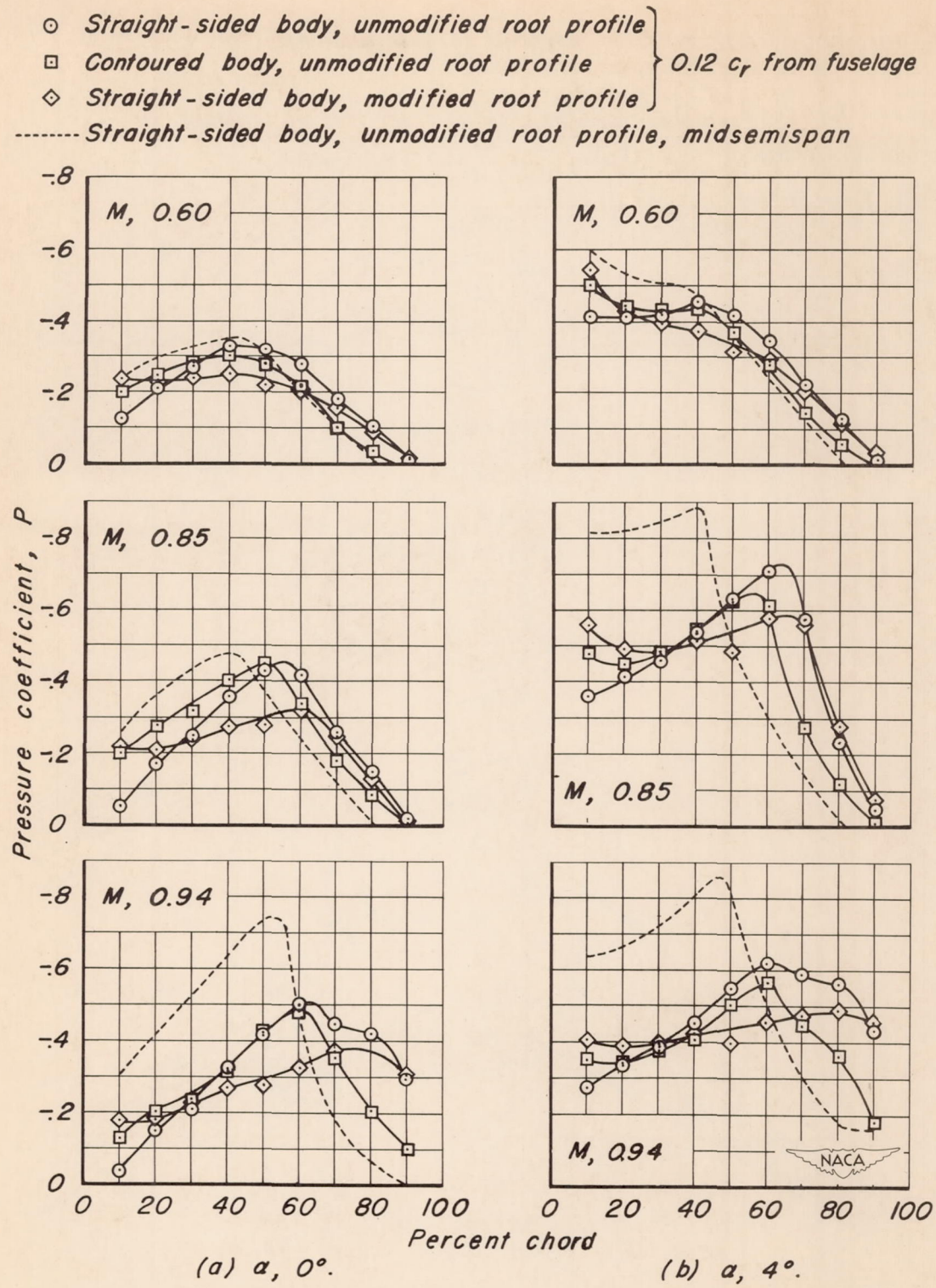

Figure 8.- Effect of model modifications on the upper-surface pressure distribution near the root of the swept wing.

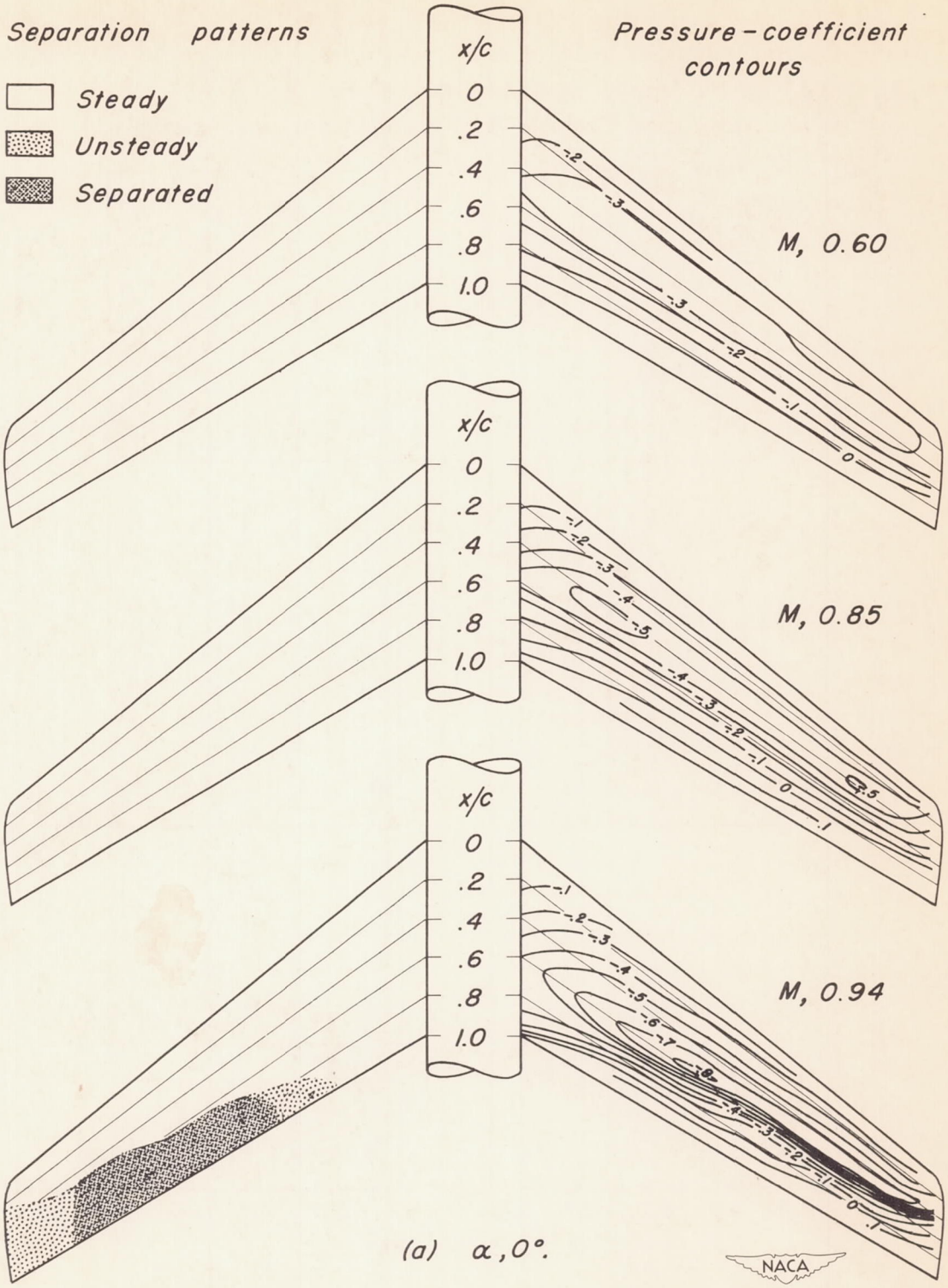

Figure 9.- Flow patterns over the swept wing with straight-sided body, unmodified root profile.

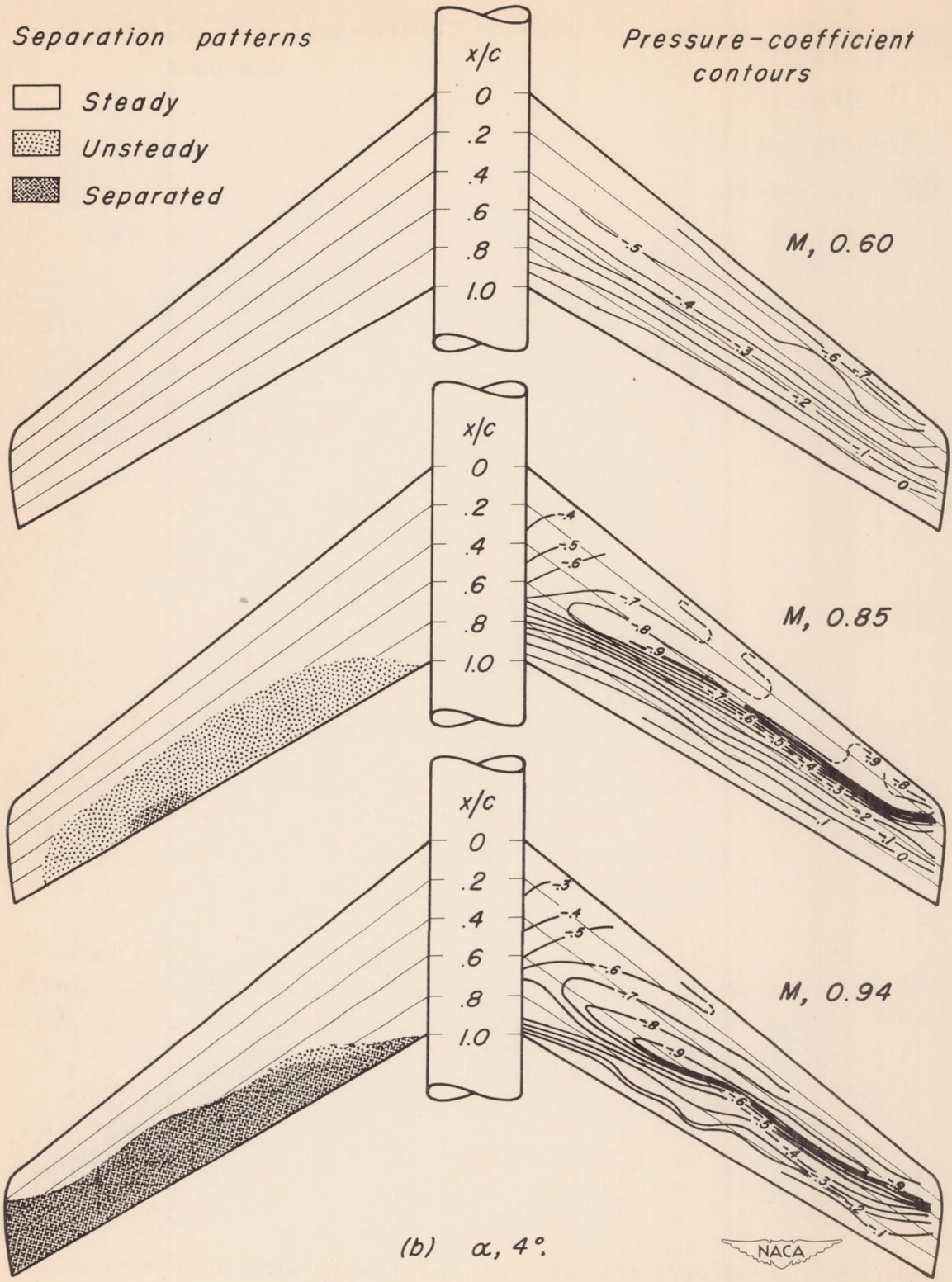

Figure 9.- Concluded.

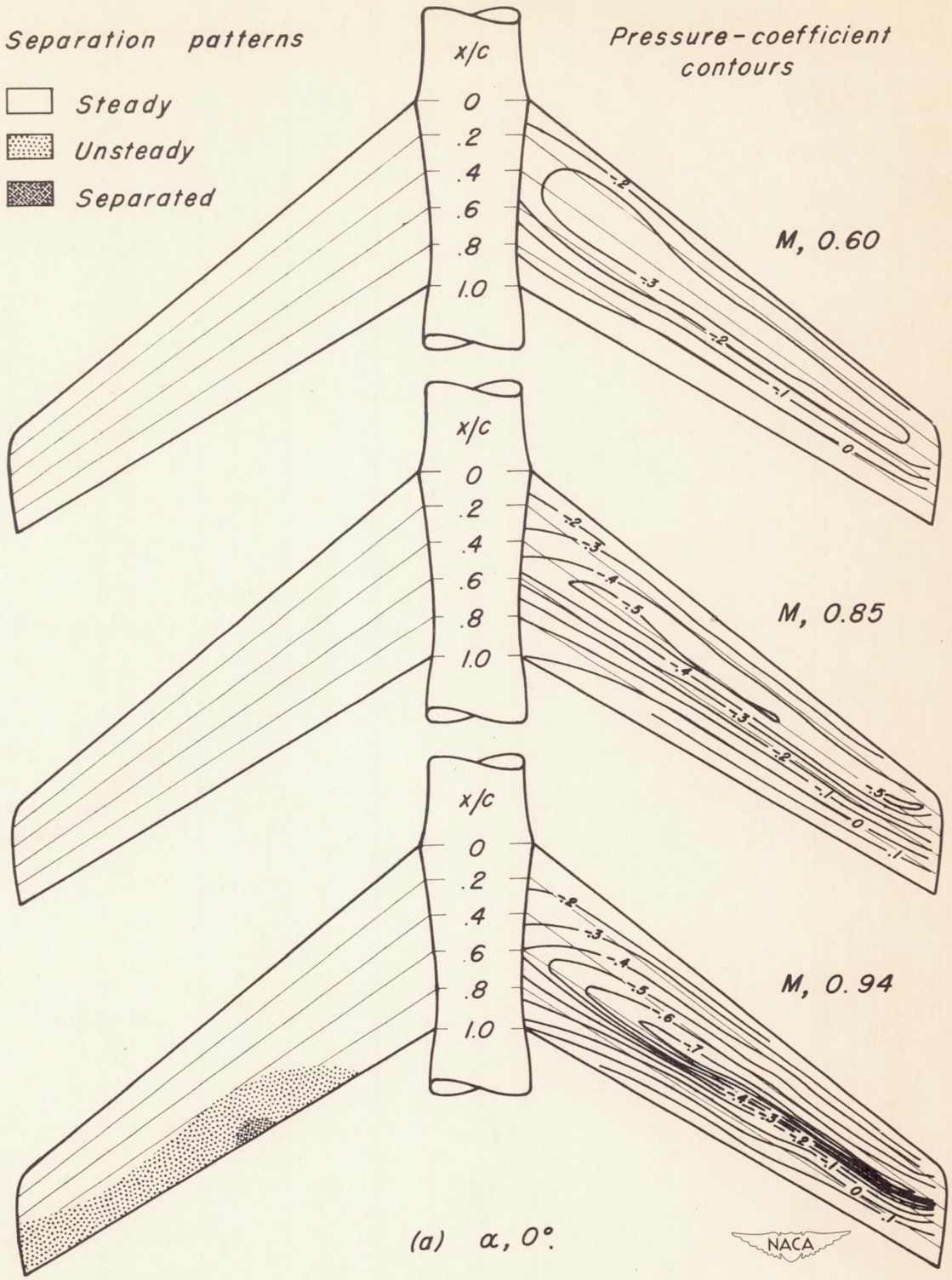

Figure 10. - Flow patterns over the swept wing with contoured body, unmodified root profile.

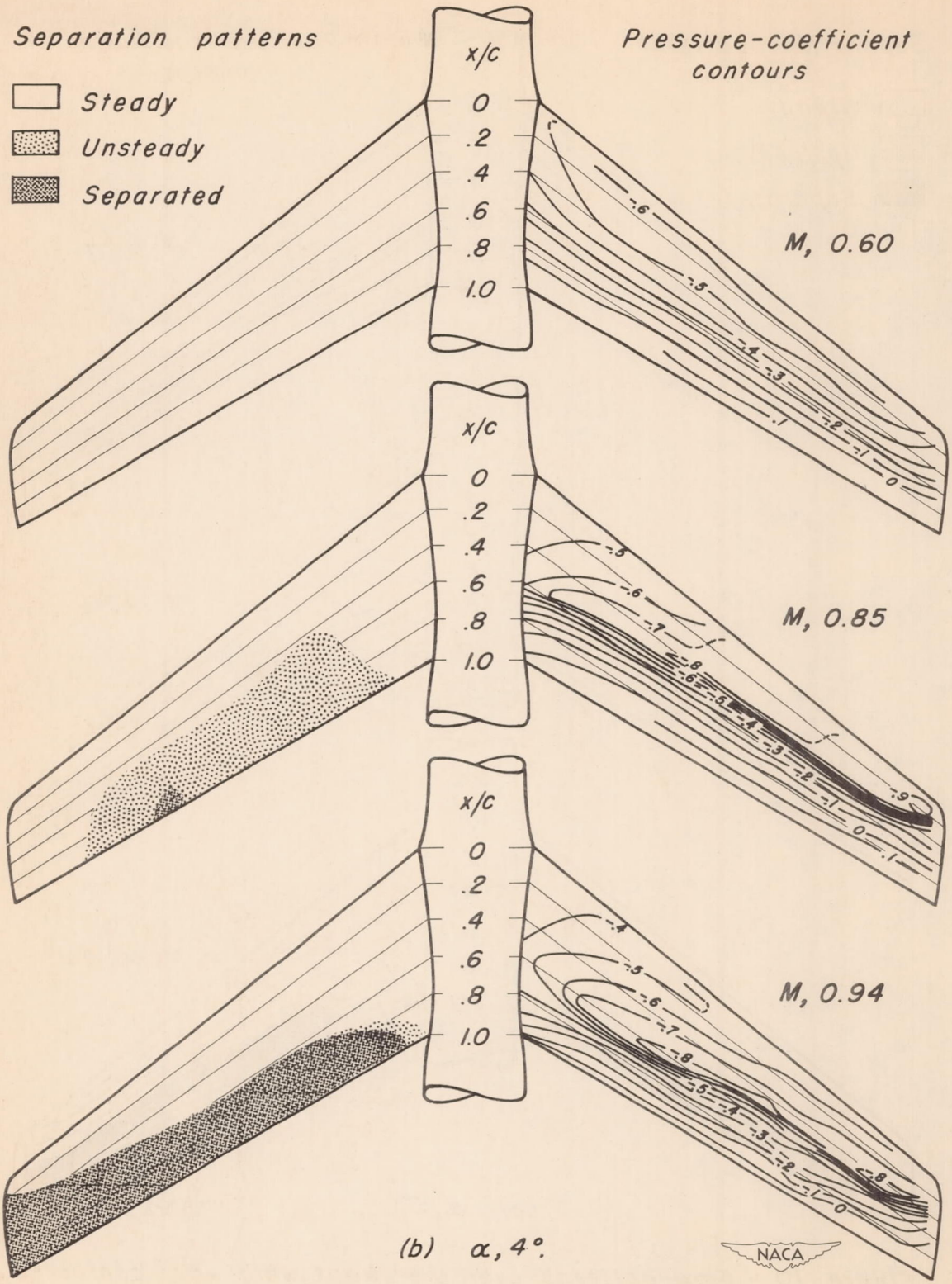

(b) α, 4°.

Figure 10.- Concluded.

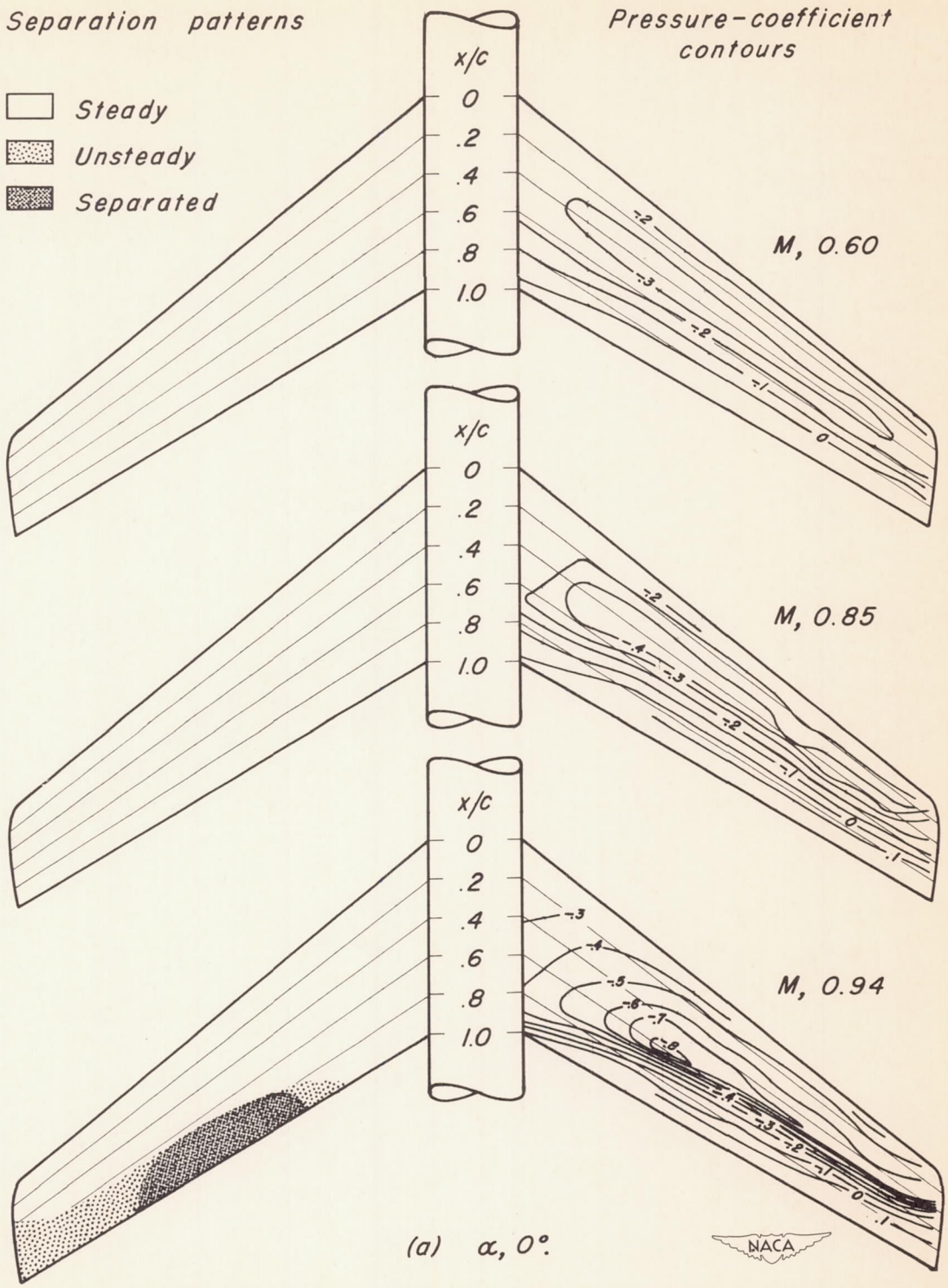

Figure 11.- Flow patterns over the swept wing with straight-sided body, modified root profile.

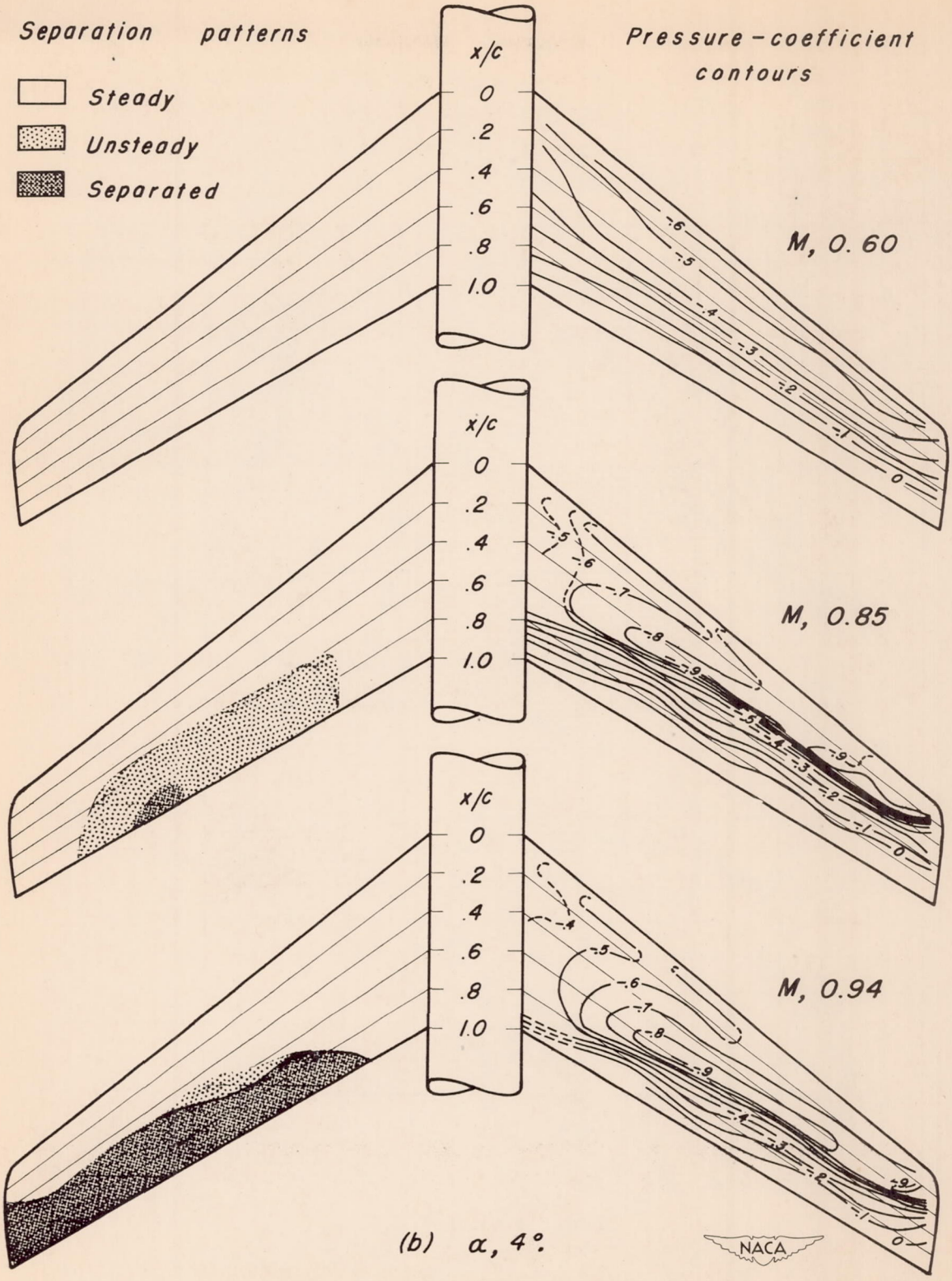

Figure 11.- Concluded.

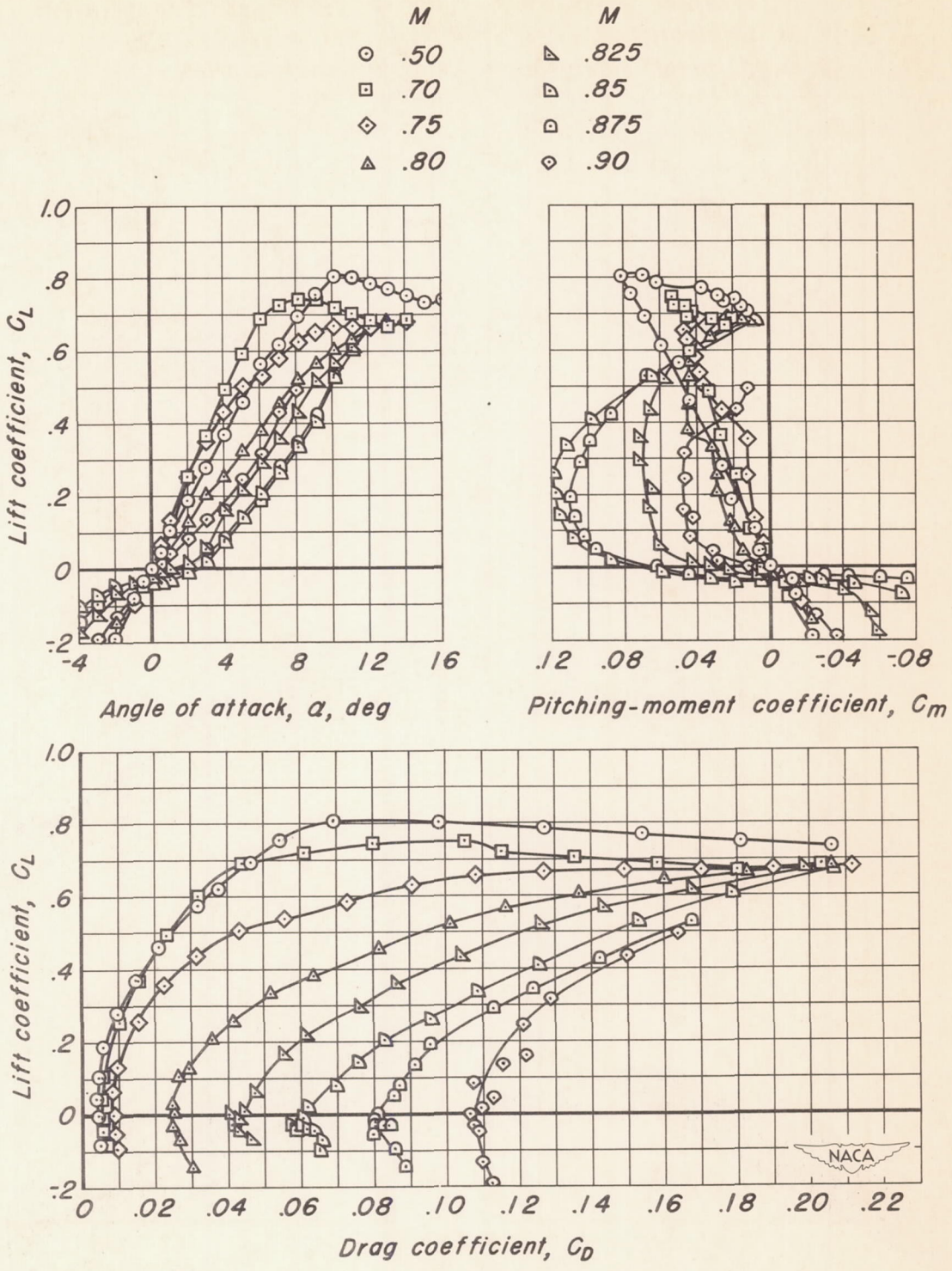

Figure 12.- Aerodynamic characteristics of the model with the unswept wing.

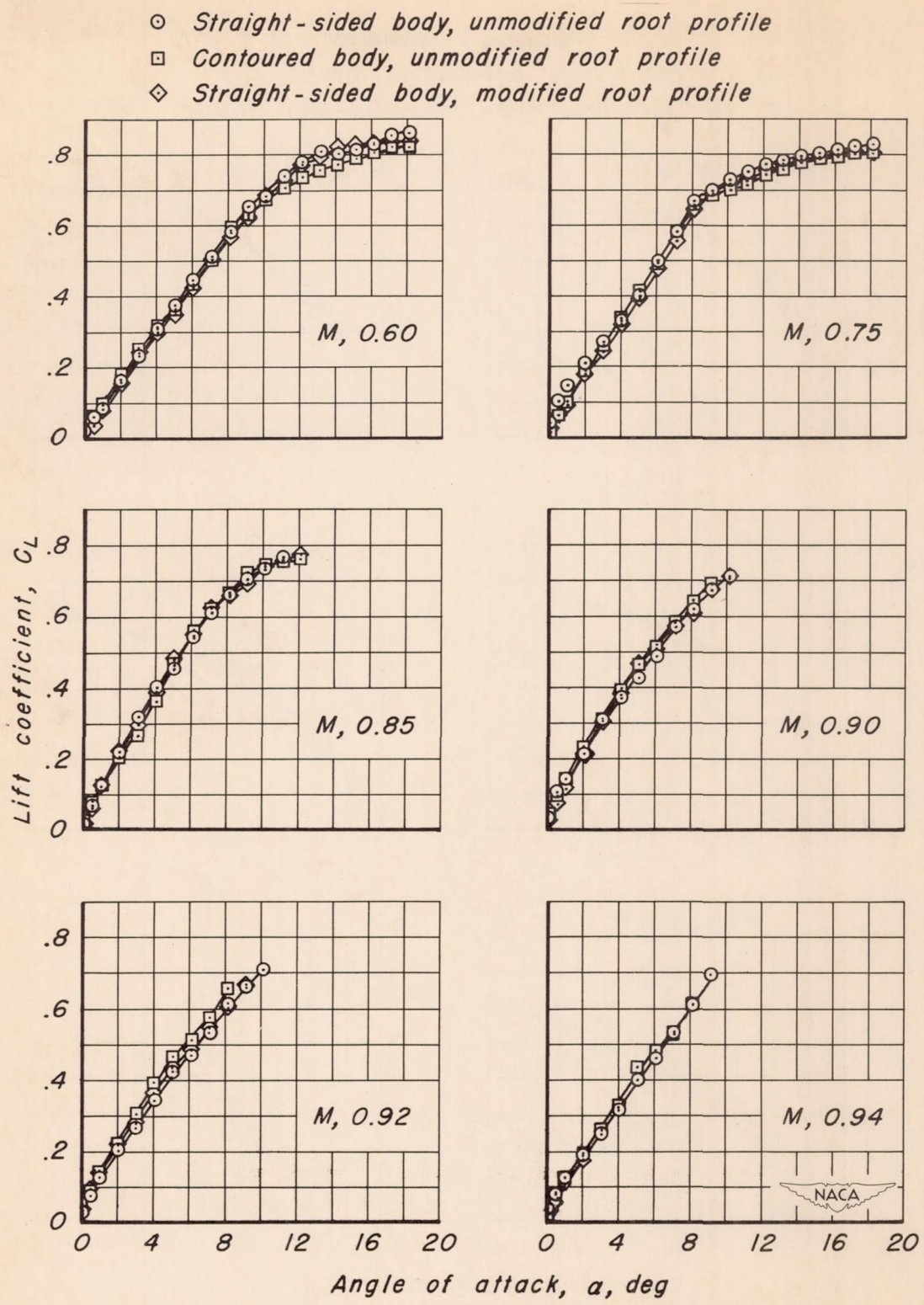

Figure 13.- Lift characteristics of the model with the swept wing.

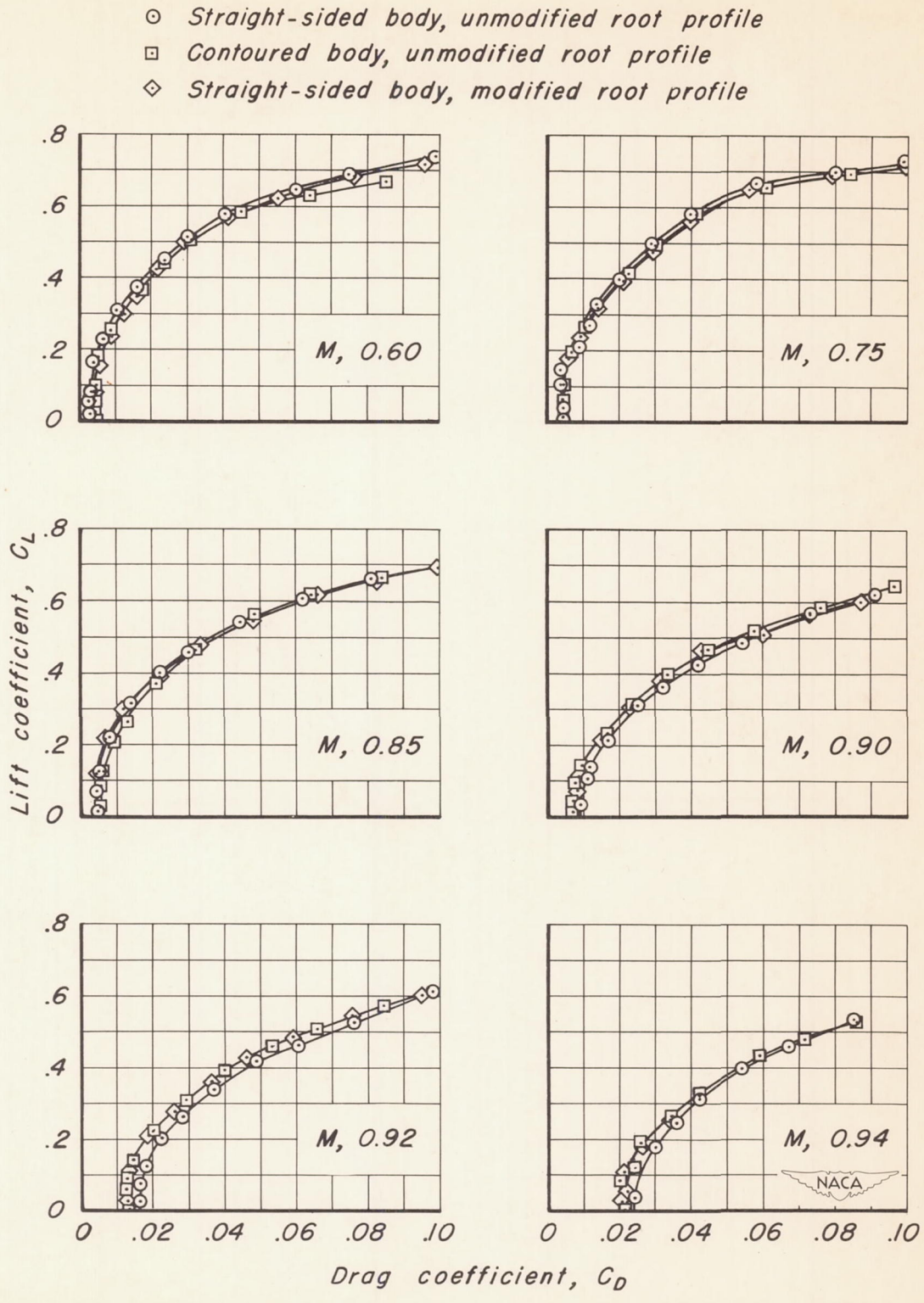

Figure 14.- Drag characteristics of the model with the swept wing.

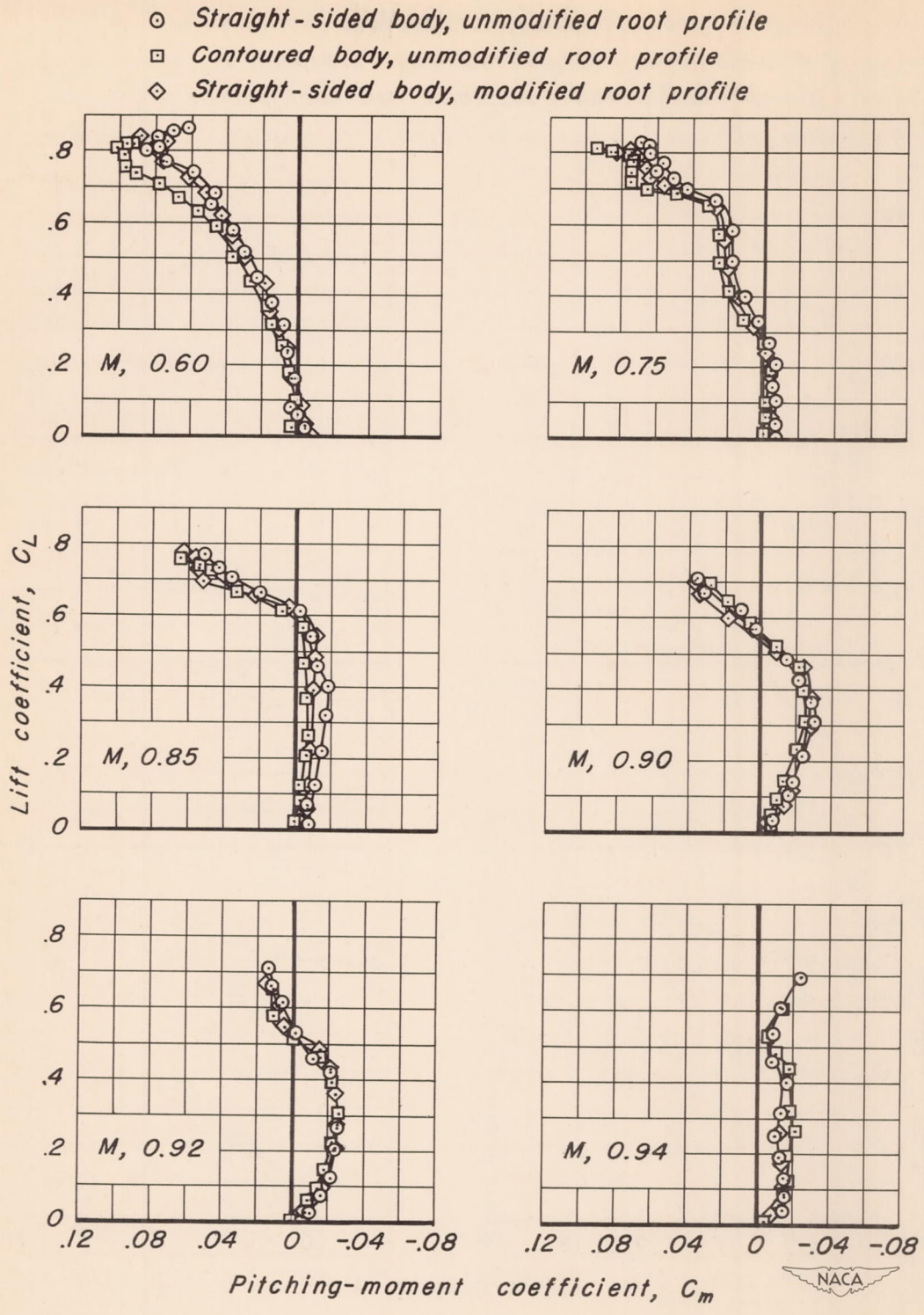

Figure 15.- Pitching-moment characteristics of the model with the swept wing.

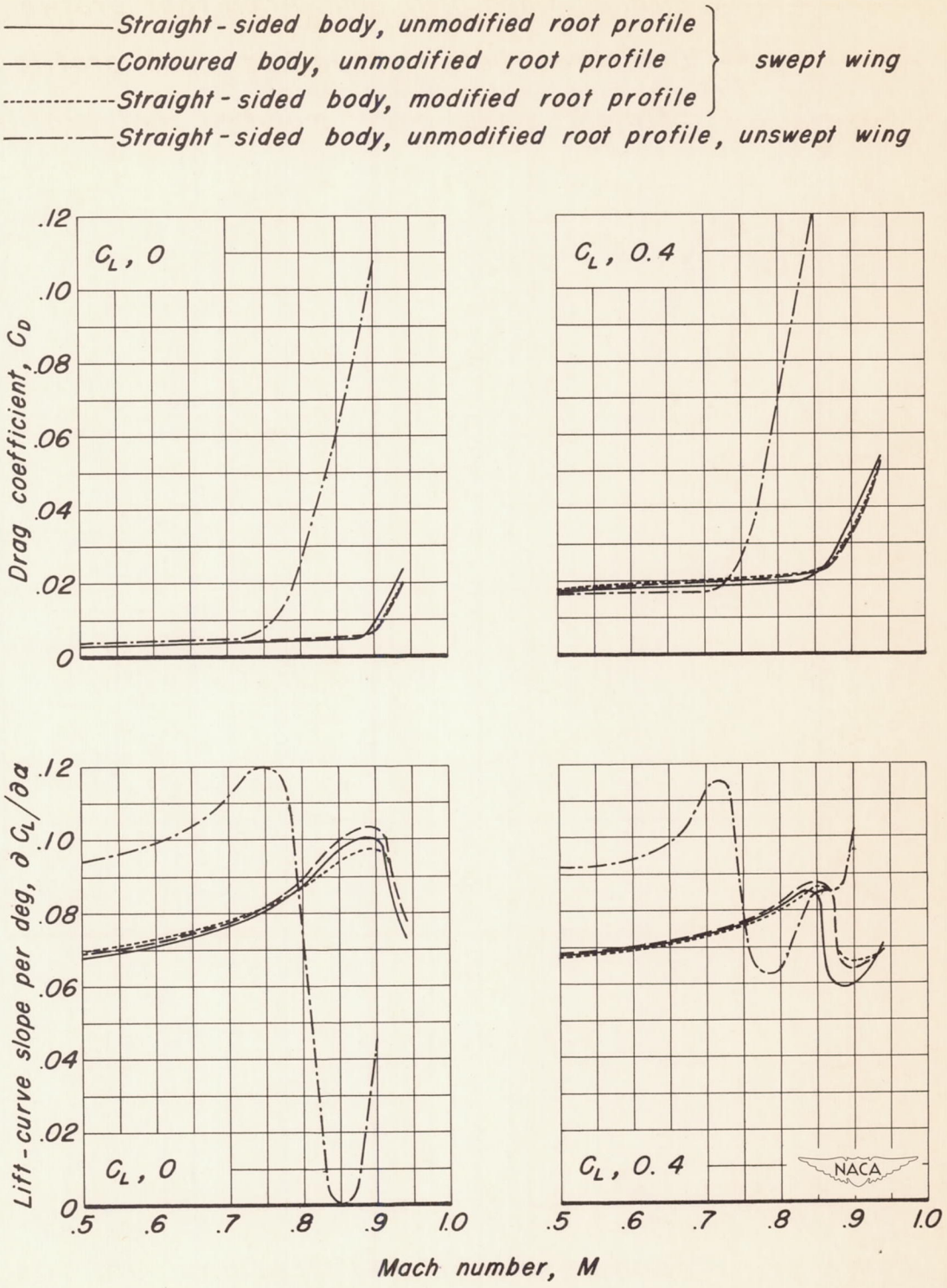

Figure 16.- Effect of Mach number on drag coefficient and lift-curve slope of the model.

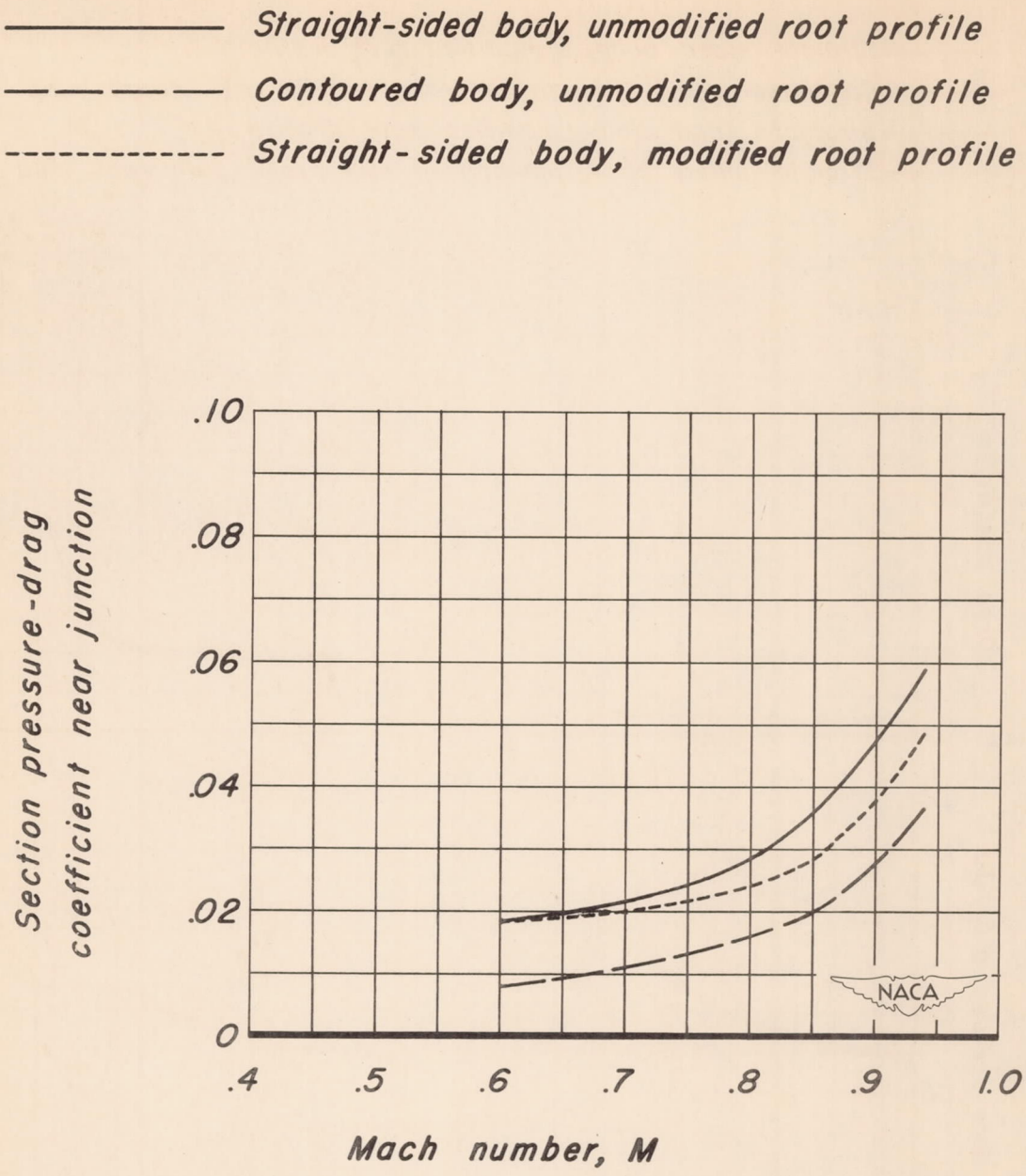

Figure 17.- Effect of model modifications on the pressure drag near the root of the swept wing for 0° angle of attack.